Organic–gold nanoparticles

DOI: 10.1002/smll.200600442

Conducting Organic–Metallic Composite Submicrometer Rods Based on Ionic Liquids**

Ashavani Kumar, Saravanababu Murugesan, Victor Pushparaj, Jin Xie, Caterina Soldano, George John, Omkaram Nalamasu, Pulickel M. Ajayan, and Robert J. Linhardt**

Molecular self-assembly is an emerging subdiscipline of material science with important potential technological applications.[1] Self-assembly is known in both molecular chemistry (for example, aggregation of molecules, molecular crystal or phase-separated polymers) and biology (for example, bilayer formation, protein folding and unfolding).[2] Molecular self-assembly typically relies on amphiphilic molecules that can be assembled into various geometric structures (for example, spherical, cylindrical, or planar) by triggering their insolubility in a medium through the adjustment of environmental conditions, such as temperature, pH value, or solvent composition. Self-assembly plays a key role in the electronics industry in the fabrication of organic memory cells. Extensive efforts have been directed at preparing nanostructures for use in memory cells, with self-assembled structures of specified size and shape containing incorporated doping materials. The main advantages of self-assembly for electronic applications are the simple, scalable, and affordable processing methods that avoid expensive lithography techniques. Various nanomaterials are being investigated to address these applications, including pyridinium salt crystals with ferroelectric properties prepared by slow evaporation.[3] Self-assembled organic-based nanostructures can show excellent electrical properties.

The synthesis of nanostructures at room temperature should improve process scalability without adversely impacting on the control over size and shape. Room-temperature ionic liquids (RTILs) are molten salts that are becoming increasingly important solvents due to their nonvolatility, thermal stability, and designable miscibility with cosolvents. RTILs have been used for various chemical reactions,[4] nanomaterials synthesis,[5] separations,[6] and electrochemical applications,[7] as well as biopolymer[8] and molecular self-assembly.[9] The synthesis of metal nanoparticles, hollow TiO_2, porous SiO_2, and CuCl platelets in RTIL solvents/templates is already known.[10] Here we demonstrate the use of an RTIL for the synthesis of pyridinium-based organic–metal composite nanostructures by electrostatically induced self-assembly. Using a simple approach, we assemble *N*-butyl-4-methylpyridinium tetrafluoroborate ([bmp][BF_4]) and chloroauric acid into hexagonal rods of Au–RTIL. This assembly results from the electrostatic complexation of the RTIL with chloroauric acid to form nanorods. Gold nanoparticles were also found embedded in these self-assembled rods, probably resulting from the photoreduction of chloroauric acid during the reaction or from reduction by ethanol during the extraction process. The aspect ratio of the Au–RTIL rods can be varied by changing the relative molar ratio of the RTIL and chloroauric acid. To our knowledge, this represents the first report of salt-assisted self-assembly of metal–organic nanostructures. The resulting rods containing gold nanoparticles are conductive and exhibit typical organic-memory-cell behavior.

Anisotropic Au–RTIL particles were obtained directly by dissolving chloroauric acid in the RTIL, as observed by scanning electron microscopy (SEM). Figure 1 A–C shows SEM images of drop-coated films of Au–RTIL after washing with ethanol. These SEM images show well-defined hexagonal rods with very smooth surface morphology. The rods are quite uniform, and the rod size, diameter, and aspect-ratio distributions are shown in Figure 1 D–F. Gaussian fits to the histograms yield an average rod length of (3 ± 1.5) μm, a diameter of (700 ± 150) nm, and an aspect ratio of 5 ± 1, respectively. There are also some fines present with the rods; these correspond to immature rods formed during the reaction.

The chemical composition of these rods was determined by X-ray photoemission electron spectroscopy (XPS). The general scan spectrum of the film at room temperature showed the presence of C 1s, N 1s, B 1s, F 1s, and Au 4f core levels with no evidence of impurities. The film was sufficiently thick and, therefore, no signal was measured from the substrate (Si 2p core level). The Au 4f spectrum was recorded from the film deposited at room temperature (Figure 2 A). The Au 4f spectrum could be resolved into a two

[*] Dr. A. Kumar, Dr. V. Pushparaj, C. Soldano, Dr. O. Nalamasu, Prof. P. M. Ajayan
Department of Material Science and Engineering
Rensselaer Polytechnic Institute
110, 8th Street, Troy, NY 12180 (USA)
Fax: (+1) 518-2768554
E-mail: pushpv@rpi.edu
Prof. R. J. Linhardt
Departments of Chemical and Biological Engineering, Biology, and Chemistry and Chemical Biology
4005 Biotech Center, Rensselaer Polytechnic Institute
110, 8th Street, Troy, NY 12180 (USA)
Fax: (+1) 518-2763405
E-mail: linhar@rpi.edu
Dr. S. Murugesan
Department of Chemical and Biological Engineering
Rensselaer Polytechnic Institute
110, 8th Street, Troy, NY 12180 (USA)
J. Xie
Department of Chemistry and Chemical Biology
Rensselaer Polytechnic Institute
110, 8th Street, Troy, NY 12180 (USA)
Dr. G. John
Department of Chemistry, City College
New York, NY 13301 (USA)

[**] We gratefully acknowledge a gift grant from Philip Morris USA through the RPI Nanotechnology Center, a seed grant from NSF-NSEC. We thank the NIH for its support through grant A11485. We also thank Dr. Subbalakshmi Sreekala (Princeton University, USA) for valuable discussions.

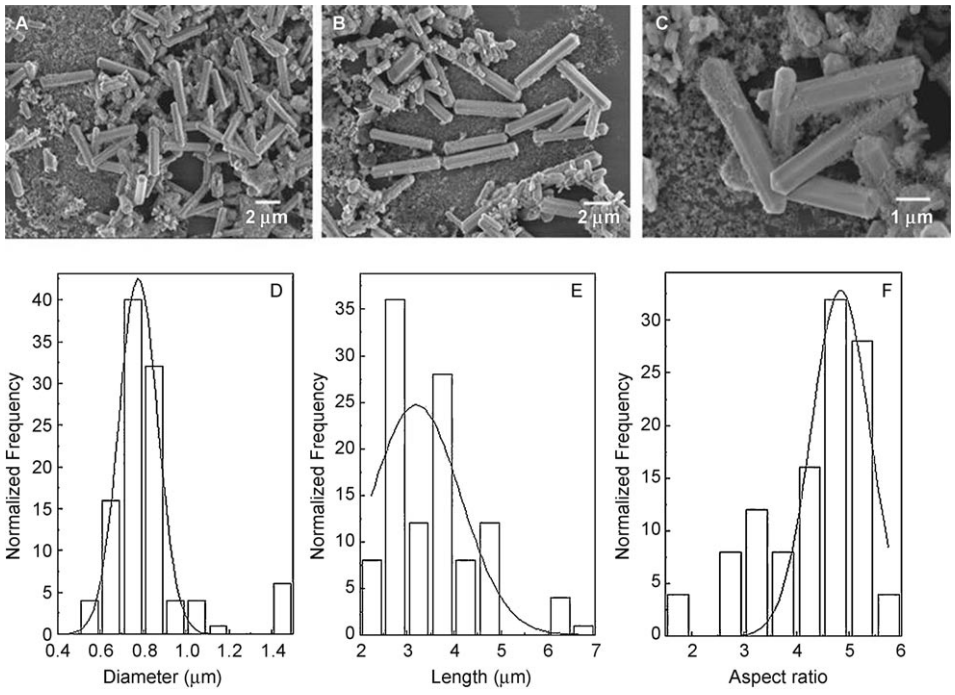

Figure 1. A–C) SEM images of Au–RTIL rods obtained with ionic liquids. D–F) Size distributions of the rods shown in A–C, respectively.

spin-orbit pair (splitting ≈ 3.7 eV) with $4f_{7/2}$ binding energies (BEs) of 83.8 and 85 eV. These components correspond to the reduced Au^0 and unreduced Au^{III} states of gold, respectively. These binding energies are in good agreement with the XPS findings of Leff et al. for alkylamine-capped gold nanoparticles.[11] The N 1s core level could be resolved in two components with binding energies of 399 and 402 eV (Figure 2B). The presence of nitrogen suggests that the nanostructure is composed of the pyridinium moiety. Two bands indicate that there are two types of nitrogen present in the film. The lower- and higher-energy components correspond to the nitrogen atoms attached to the Au^0 and Au^{III} and to the protonated nitrogen atoms present in the ionic-liquid species. In addition to gold, B 1s, Cl 2p, and F 1s core levels are also observed in the film (data not shown), a result suggesting the presence of both $[BF_4]^-$ and $[AuCl_4]^-$ ions. The presence of metallic gold, observed in the XPS study, suggests the formation of metal nanoparticles. Metal nanoparticles are known to show characteristic absorbance in the visible region due to excitation of surface plasmon vibrations. A UV/Vis measurement, carried out on a drop-coated film of rods, showed absorption bands at 500, 800, and 1080 nm (Figure 2C). This absorbance pattern is characteristic of the surface plasmon resonance (SPR) of gold nanoparticles and confirms the presence of gold nanoparticles in the hexagonal rods. The peaks at 500 and 800 nm correspond to transverse and longitudinal components of the surface plasmon resonance of gold nanoparticles, respectively. The peak at 1080 nm may be due to quadrupole and higher multipole plasma excitation.[12] Both visible and XPS spectroscopy confirm that the rods are composed of gold nanoparticles, gold ions, chloride ions, and ionic liquid ([bmp][BF_4]). A TEM image of the gold nanoparticles is shown in Figure 2D. It is clear that the particles are well defined and discrete; the image confirms the presence of metallic gold nanoparticles with sizes ranging from 20–40 nm. This observation is in agreement with the other characterizations.

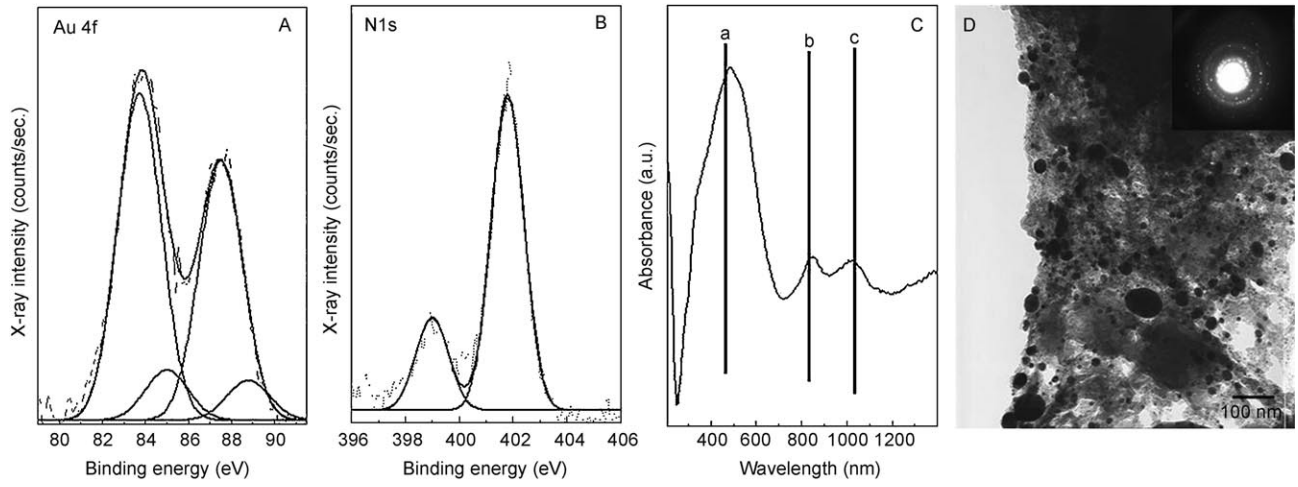

Figure 2. A, B) Au 4f and N 1s core-level spectra recorded from a Au–RTIL film grown on a Si(111) substrate. C) UV/Visible spectrum obtained from the drop-coated film of rods. D) Transmission electron microscopy (TEM) image of a drop-coated film of the Au–RTIL solution on a carbon-coated grid (inset: diffraction pattern of gold).

The composition of the rods was further characterized by analyzing the residual reaction solution by ^{1}H NMR spectroscopy and the rods by electrospray-ionization mass spectrometry (ESI-MS). The reaction mixture was centrifuged at 9500 rpm for 5 min to separate the rods from the residual solution. The residual solution was dissolved in CD_3OD and subjected to ^{1}H NMR analysis. The ^{1}H NMR spectra of the starting material ([bmp][BF_4]) and the residual solution showed identical peaks (^{1}H NMR (CD_3OD): $\delta = 9.75$ (d, 2H, $J \approx 6.84$ Hz), 8.90 (d, 2H, $J \approx 6.35$ Hz), 5.53 (t, 2H), 3.66 (s, 3H), 2.95 (m, 2H), 2.39 (m, 2H), 1.98 ppm (t, 3H)). The RTIL (1-butyl-4-methylpyridinium cation), while still clearly comprising the bulk of the residual solution, was reduced in comparison to the pure RTIL starting material, a fact suggesting that the RTIL was consumed with the formation of the organic nanorod composites. The rods, collected by centrifuging the reaction mixture, were washed with ethanol, suspended in ethanol, and analyzed by ESI-MS. A peak corresponding to the RTIL cation [bmp] ($m/z = 150$) and another peak ($m/z = 387$) corresponding to the complex [bmp]$_2$[BF_4] were the major peaks observed in the positive-ion mode of ESI-MS. The negative-ion mode of the ESI-MS analysis showed a prominent peak ($m/z = 338.7$) corresponding to [$AuCl_4$]$^-$ ions. These observations confirm the presence of both the RTIL and [$AuCl_4$]$^-$ ions electrostatically complexed within the rods.

The XPS, NMR, MS, and visible-spectra analyses clearly indicate that the RTIL was not involved in the reduction process of Au^{III} and that the rods were composed of pyridinium ions, chloroaurate ions, tetrafluoroborate ions, and gold nanoparticles. Pyridinium–[$AuCl_4$]$^-$ complexes have previously been used for the synthesis of gold nanoparticles and the gold ions present in these nanoparticles were very prone to photoreduction.[13] This suggests that photoreduction might also be responsible for the formation of the gold nanoparticles entrapped in our composite hexagonal rods.

Careful analysis of these rods was carried out by using SEM to understand the assembly mechanism behind the formation of the hexagonal rods. Figure 3 shows SEM images of immature crystals obtained from different parts of the same sample. These SEM images can be used to understand the sequence of growth of these nanostructures (Figure 3A–F). Figure 3A shows the randomly oriented rods of composite materials. Organic molecules of hexagonal conformation are known to stack upon one another to form nanorods; furthermore, these nanorods can self-organize into larger aggregates with similar appearance.[14] In the current case, we believe that the pyridinium cations complexed to gold(III)/chloride/[BF_4]$^-$ ions stack upon one another and assemble in rodlike macrostructures. This observation is consistent with the reported capability of ionic liquids to act as entropic drivers in the formation of self-organized and well-defined nanomaterials with extended order.[15] The progressive self-assembly of these rods into well-defined bundles can be seen in Figure 3B–D. Figure 3E shows the immature hexagonal rods clearly displaying thin rods protruding from large hexagonal bundles. The final aggregated bundles of hexagonal Au–RTIL rods develop a smooth surface through the deposition of excess gold–RTIL complex, which fills in the gaps between the individual rods (Figure 3F).

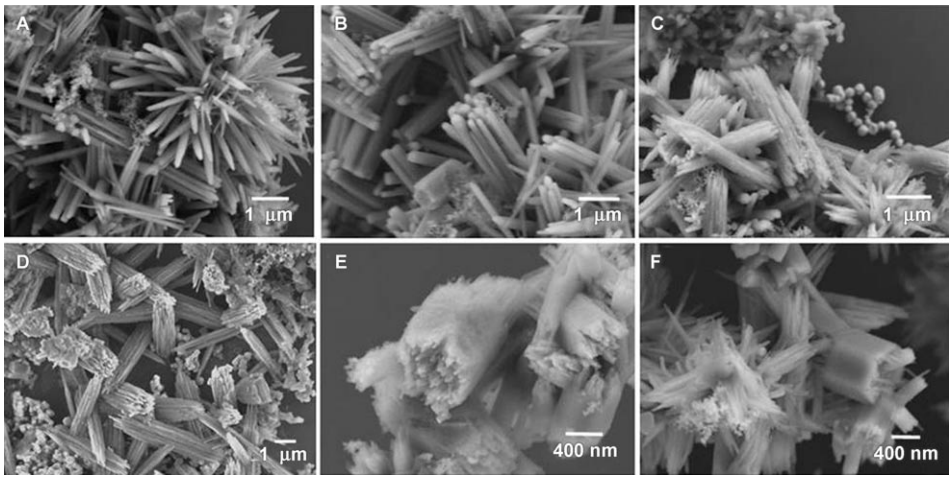

Figure 3. Growth mechanism of anisotropic hexagonal organic–metallic nanorods.

The size of the aggregates depends on the relative amount of chloroauric acid and ionic liquid. To demonstrate this concentration-dependent size effect, similar experiments were carried out with variation in the molar ratio of chloroauric acid and RTIL. At lower molar ratios of chloroauric acid and ionic liquid ($HAuCl_4$:RTIL = 1:4), the size of the rods ranged from 10–50 μm with a diameter of ≈1 μm, thereby giving a high aspect ratio (Figure 4A). An increase in the molar ratio ($HAuCl_4$:RTIL = 1:130) results in the formation of hexagonal-shaped particles with high polydispersity, as shown in Figure 4B. These particles clearly show hexagonal facets and a thickness of ≈200 nm. Thus, the present method is efficient for obtaining rods of the desired aspect ratio just by adjusting the chloroauric acid concentration. Since these rods are composed of gold nanoparticles and organic ions, these rods were tested to determine whether they show interesting electrical properties.

The electrical properties of these rods were determined by measuring their current–voltage (I–V) characteristics. The Au–RTIL rods were well dispersed on the SiO_2/Si substrate, and a metal electrode (platinum; bottom inset of Figure 5) was deposited on each individual rod by using the focused ion beam technique (ZEISS 1540XB CrossBeam Series apparatus). Deposited coplanar metal electrodes were used to measure the I–V characteristics. The current–voltage characteristics showed a nonlinear and asymmetrical behavior in the dc bias-swept regime (Figure 5). The top inset of Figure 5 shows the direction of the voltage bias swept back and forth. The bias is swept from 0–100 V (a)

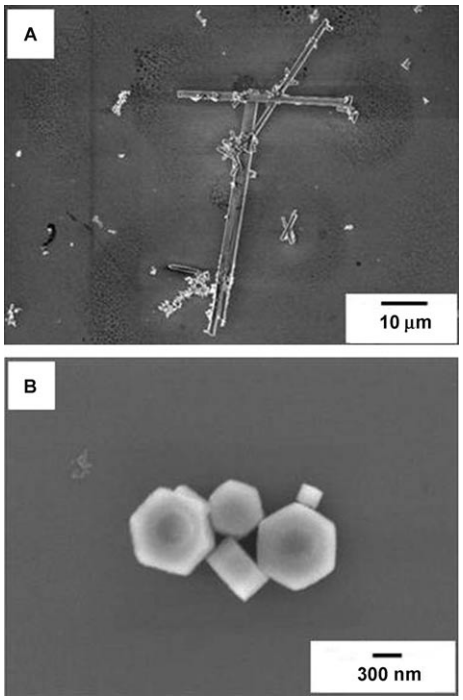

Figure 4. SEM images of hexagonal rods obtained by using an ionic liquid at A) 1:4 molar ratio and B) 1:130 molar ratio.

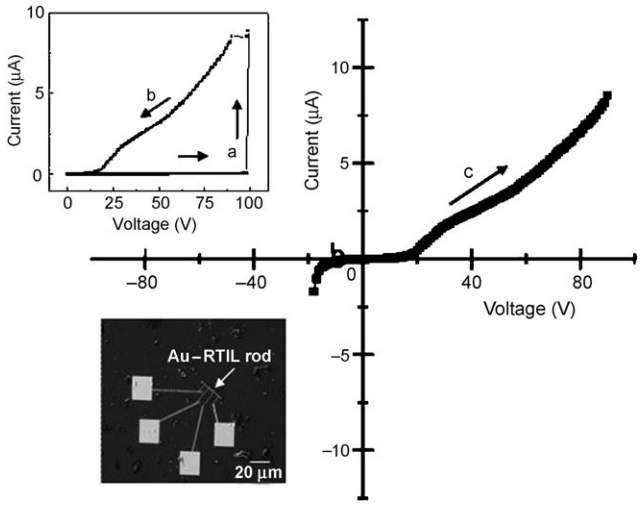

Figure 5. Current–voltage (*I–V*) characteristics of a single hexagonal Au–RTIL rod obtained from the second scan forwards. The top inset shows the *I–V* curves obtained during the first scan forth and back. The bottom inset shows the SEM image of the Pt electrodes deposited on the Au–RTIL rod. The square pads are the Pt electrodes.

and swept back to 0 (b); the subsequent scan is shown as (c). The *I–V* curve (top inset of Figure 5) swept in the first scan forth and back displayed a large hysteresis behavior. The current measured during the first scan (a) at 50 V was 8 nA, while the measured current at 50 V on sweeping back (b) was 3 μA; this displays a transition from the lower to higher current with nearly three orders of current change. This transition was observed only at higher voltages and the higher current was repeatable in subsequent sweeps after the initial first scan. The *I–V* behavior obtained in our device is similar to the organic-memory-cell behavior called WORM (write once, read many times).[16–18] By using platinum electrodes and sweeping from one contact pad to the other (and vice versa), the same asymmetrical *I–V* behavior was observed. The behavior remained unchanged even when the electrodes were changed from platinum to tungsten. No linear relationship was observed between $\log I$ and $V^{1/2}$ in any of the voltage regimes, a result indicating that the current was not controlled by charge injection from the Pt electrode into the hexagonal rod. These data clearly indicate that the hexagonal rod alone was responsible for the major contribution in the electrical conduction. There is also a possibility that electric-field-induced polarization in a specific direction can occur in the hexagonal rod, which can result in asymmetric behavior. The presence of the Au nanoparticles in the synthesized rods can induce charge transfer between Au nanoparticles and the RTIL present in the complex, thereby orienting the dipoles along one direction. The synthesized rod device displays excellent stability through many cycles and represents a promising candidate for an organic memory cell.

In summary, we have successfully assembled organic–metallic hexagonal rods by a simple, electrostatic complexation of an RTIL and chloroauric acid ions. The gold ions entrapped in these rods get reduced and form nanoparticles. The aspect ratio of the obtained structures can be tuned by changing the relative concentration of the RTIL and chloroauric acid. These hexagonal rods exhibit asymmetric and hysteretic *I–V* behavior and are prime candidates for organic memory cells.

Experimental Section

Chloroauric acid and [bmp][BF_4] were obtained from Aldrich (St. Louis, MO) and used without further purification.

Preparation of pyridinium-based nanostructures: In a typical experiment, chloroauric acid (0.127 g) was dissolved in the RTIL [bmp][BF_4] (1.98 g). The RTIL became turbid and a white precipitate was seen in the reaction mixture upon addition of the chloroauric acid. Drop-coated films of this dispersion were prepared on silicon wafers by using a spin coater. The resulting films were immersed in ethanol for 1 h to remove excess RTIL prior to characterization.

Characterization: Visible spectroscopy, IR spectroscopy, X-ray photoemission spectroscopy, and FESEM were used to characterize the reaction product. Visible spectroscopy measurements of all films were performed on a Perkin–Elmer Lamda 950 spectrophotometer operated at a resolution of 2 nm. The morphology of the nanostructures was characterized by SEM by using a JEOL 6330 F FESEM microscope operated at 5 kV. X-ray photoelectron spectroscopy measurements were carried out in a PHI 5400 instrument with a 200 W Mg Kα probe beam. The spectrometer was configured to operate at high resolution with a pass energy of 20 eV. For TEM analysis, rods were dissolved in excess ethanol by using sonication and the solution was drop coated as a film on carbon-coated grids for TEM analysis.

The electrodes deposited on the individual Au–RTIL rod (≈25 μm) were prepared by the focused ion beam technique (ZEISS 1540XB CrossBeam instrument) for the electrical measurement (inset of Figure 5). Deposition of the metal was carried at different current ratings (100 pA–1 nA at 30 kV) depending on the part of the electrode to be deposited. The deposition current was 100 pA for deposition on the individual Au–RTIL rods so as not to damage the sample, while the larger area square pads (50–300 μm^2) on the SiO_2/Si substrate were deposited at 1 nA. All the electrode (Pt) deposition was carried out at 2×10^{-6} torr. The current–voltage measurement was carried out by using a Keithley 6430 apparatus interfaced with a computer for data acquisition. The rods were also studied by ^{1}H NMR spectroscopy and ESI-MS for chemical characterization.

Keywords:
conducting materials · gold · ionic liquids · nanoparticles · organic–metallic complexes

[1] M. Boncheva, D. A. Bruzewicz, G. M. Whitesides, *Pure Appl. Chem.* **2003**, *75*, 621 – 630.
[2] a) J. M. Lehn, P. Ball in *The New Chemistry* (Ed.: N. Hall), Cambridge University Press, Cambridge, UK, **2000**, pp. 300—351; b) E. L. Thomas, *Science* **1999**, *286*, 1307 – 1309; c) P. Bongrand, *Rep. Prog. Phys.* **1999**, *62*, 921 – 968; d) V. Grantcharova, E. J. Alm, D. Baker, A. L. Horwich, *Curr. Opin. Struct. Biol.* **2001**, *11*, 70 – 82.
[3] P. Czarnecki, I. Szafraniak, *Phys. Status Solidi B* **1998**, *209*, 211 – 220.
[4] T. Welton, *Chem. Rev.* **1999**, *99*, 2071 – 2084.
[5] a) M. Antonietti, D. Kuang, B. Smarsly, Y. Zhou, *Angew. Chem.* **2004**, *116*, 5096 – 5100; *Angew. Chem. Int. Ed.* **2004**, *43*, 4988 – 4992; b) J. Dupont, G. S. Fonseca, A. P. Umpierre, P. F. P. Fichtner, S. R. Teixeira, *J. Am. Chem. Soc.* **2002**, *124*, 4228 – 4229.
[6] J. G. Huddleston, H. D. Willauer, R. P. Swatloski, A. E. Visser, R. D. Rogers, *Chem. Commun.* **1998**, 1765 – 1766.
[7] E. V. Dickinson, M. E. Williams, S. M. Hendrickson, H. Masui, R. W. Murray, *J. Am. Chem. Soc.* **1999**, *121*, 613 – 616.
[8] N. Kimizuka, T. Nakashima, *Langmuir* **2001**, *17*, 6759 – 6761.
[9] T. Nakashima, N. Kimizuka, *Chem. Lett.* **2002**, *31*, 1018 – 1020.
[10] a) T. Nakashima, N. J. Kimizuka, *J. Am. Chem. Soc.* **2003**, *125*, 6386 – 6387; b) A. Taubert, *Acta Chim. Slov.* **2005**, *52*, 168 – 170; c) Y. Zhou, M. Antonietti, *J. Am. Chem. Soc.* **2003**, *125*, 14960 – 14961.
[11] D. V. Leff, L. Brandt, J. R. Heath, *Langmuir* **1996**, *12*, 4723 – 4730.
[12] R. Jin, Y. W. Cao, C. A. Mirkin, K. L. Kelly, G. C. Schatz, J. G. Zheng, *Science* **2001**, *294*, 1901 – 1903.
[13] K. Torigoe, K. Esumi, *Langmuir*, **1992**, *8*, 59 – 63.
[14] S. Leclair, P. Baillargeon, R. Skouta, D. Gauthier, Y. Zhao, Y. L. Dory, *Angew. Chem.* **2004**, *116*, 353 – 357; *Angew. Chem. Int. Ed.* **2004**, *43*, 349 – 353.
[15] J. Dupont, P. A. Z. Saurez, *Phys. Chem. Chem. Phys.* **2006**, *8*, 2441 – 2452.
[16] S. Moller, C. Perlov, W. Jackson, C. Taussig S. R. Forrest, *Nature* **2003**, *426*, 166 – 169.
[17] J. Ouyang, C. W. Chu, D. Sieves, Y. Yang, *Appl. Phys. Lett.* **2005**, *86*, 123 507 – 123 509.
[18] J. Ouyang, C. Chu, C. Szmanda, Y. Yang, *Nat. Mater.* **2004**, *3*, 918 – 922.

Received: August 22, 2006
Published online on January 30, 2007

